Biodegradable Nanoparticles Combining Cancer Cell Targeting and Anti-Angiogenic Activity for Synergistic Chemotherapy in Epithelial Cancer

Francesca moret
Padua University: Universita degli Studi di Padova
Claudia Conte
Universita degli Studi di Napoli Federico II Dipartimento di Farmacia
Diletta Esposito
Universita degli Studi di Napoli Federico II Dipartimento di Farmacia
Giovanni Dal Poggetto
IPCB CNR: Istituto dei Polimeri Compositi e Biomateriali Consiglio Nazionale delle Ricerche
Concetta Avitabile
Istituto di Biostrutture e Bioimmagini Consiglio Nazionale delle Ricerche
Francesca Ungaro
Universita degli Studi di Napoli Federico II Dipartimento di Farmacia
Natascia Tlso
Universita degli Studi di Padova
Alessandra Romanelli
Università degli Studi di Milano: Universita degli Studi di Milano
Paola Laurienzo
IPCB CNR: Istituto dei Polimeri Compositi e Biomateriali Consiglio Nazionale delle Ricerche
Elena Reddi
Universita degli Studi di Padova
Fabiana Quaglia (quaglia@unina.it)
Universita degli Studi di Napoli Federico II Dipartimento di Farmacia https://orcid.org/0000-0001-6223-0782

Research Article

Keywords: polymeric nanoparticles, anti-angiogenic peptides, folate targeting, tumor spheroids, xenografted zebrafish embryos.

Posted Date: September 14th, 2021

DOI: https://doi.org/10.21203/rs.3.rs-879223/v1

Version of Record: A version of this preprint was published at Drug Delivery and Translational Research on January 1st, 2022. See the published version at https://doi.org/10.1007/s13346-021-01090-6.

Biodegradable nanoparticles combining cancer cell targeting and anti-angiogenic activity for synergistic chemotherapy in epithelial cancer†

Francesca Moret,[a,#] Claudia Conte,[b,#] Diletta Esposito,[b] Giovanni Dal Poggetto,[c] Concetta Avitabile,[d] Francesca Ungaro, [b] Natascia Tiso,[a] Alessandra Romanelli,[e] Paola Laurienzo,[c] Elena Reddi [a,*] and Fabiana Quaglia[b,c*]

[a] Department of Biology, University of Padova, 35121 Padova, Italy

[b] Department of Pharmacy, University of Napoli Federico II, 80131 Napoli, Italy

[c] Institute for Polymers, Composites and Biomaterials, CNR, 80078 Pozzuoli, Italy;

[d] Institute of Biostructure and Bioimaging, CNR, 80134 Napoli, Italy

[e] Department of Pharmaceutical Sciences, University of Milan, 20133 Milano, Italy

[#] equally contributed

* Corresponding authors

quaglia@unina.it (F. Quaglia), elena.reddi@unipd.it (E. Reddi)

Abstract

A biodegradable engineered nanoplatform combining anti-angiogenic activity and targeting of cancer cells to improve the anticancer activity of docetaxel (DTX) is here proposed. Indeed, we have developed biodegradable nanoparticles (NPs) of poly(ethylene glycol)-poly(ε-caprolactone), exposing on the surface both folate motifs (Fol) for recognition in cells overexpressing Folate Receptor-α (FRα) and the anti-angiogenic hexapeptide aFLT1. The presence of Fol on NPs did not impair the anti-angiogenic activity of aFLT1, as assessed by *in vitro* tube formation assay in HUVEC endothelial cells. In both 2D and 3D KB cell cultures *in vitro*, the cytotoxicity of DTX loaded in NPs was not significantly affected by Fol/aFLT1 double decoration as compared to free DTX. Remarkably, NPs distributed differently in 3D multicellular spheroids of FRα-positive KB cancer cells depending on the type of ligand displayed on the surface. When tested *in vivo* in zebrafish embryos xenografted with KB cells, NPs displaying Fol/aFLT1 reduced DTX systemic toxicity and inhibited in a synergistic way the growth of the tumor mass and associated vasculature. Overall, nanotechnology offers excellent ground for combining therapeutic concepts in cancer, paving the way to the development of novel multifunctional nanopharmaceuticals where surface decoration with bioactive elements can significantly improve therapeutic outcomes.

Keywords: polymeric nanoparticles, anti-angiogenic peptides, folate targeting, tumor spheroids, xenografted zebrafish embryos.

Graphical Abstract

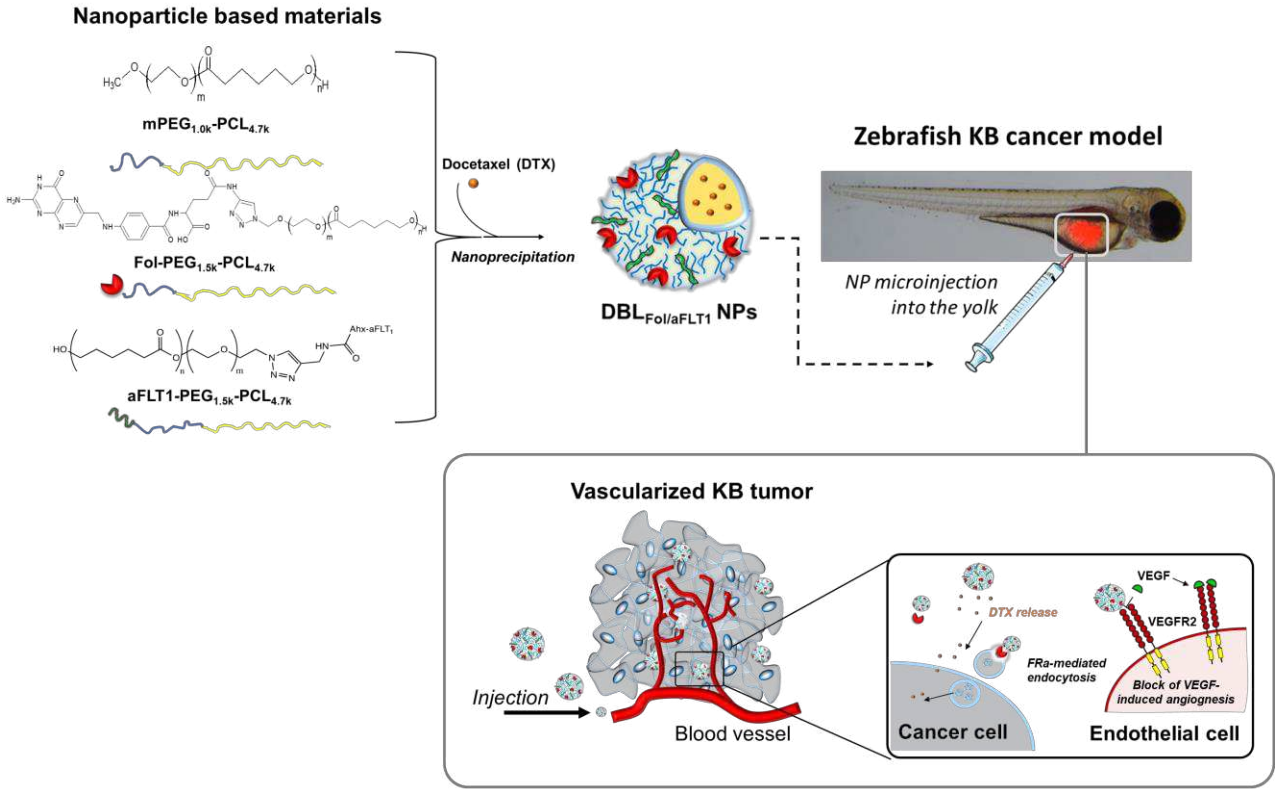

1. Introduction

In the vast arena of nanoplatforms developed so far for the delivery of chemotherapeutics, multifunctional polymeric nanoparticles (NPs) bearing different elements in a single entity offer an unprecedented tool of innovation.[1-4] This type of NPs can be engineered: i) to transport the chemotherapeutic in the desired pathological area; ii) to target specific cell population in the tumor microenvironment; iii) to deliver multiple drugs and attain synergic/additive effects.

Amphiphilic diblock copolymers of poly(ethylene glycol) and polyesters are biocompatible and biodegradable versatile materials able to form a wide range of core-shell nanostructures and to deliver multiple drugs in a sustained manner.[5-7] The presence of an outer PEG fringe makes the surface hydrophilic, which is useful to limit some undesired interactions with the biophase (opsonization in the blood compartment)[8] and to facilitate transport through mucosal tissues or extracellular matrix.[9-11] PEGylation is a two swords strategy since the benefits mentioned above are coupled with an impaired attitude of NPs to cross the cell membrane and deliver drug cargo inside cells.[12] For these reasons, surface-modification of NPs with ligands binding cell membrane receptors has been attempted to improve their selective internalization in specific cell types of tumor microsystem.[3, 13]

Folate Receptor-α (FRα) is one of the most studied surface receptor employed to this purpose since it is overexpressed in several cancer types.[14] However, the control over Folate (Fol) exposure on NPs surface is not trivial at all, [15] and poorly investigated when assembling NPs from all in one block copolymers.[13, 16] We have recently proposed different strategies for the effective display of Fol motifs on the surface of PEGylated NPs through appropriate tailoring of polymer block lengths and fabrication conditions.[16-18] Results have demonstrated a certain degree of specificity of the NPs for cancer cells overexpressing FRα, although no gain in cytotoxicity was observed.

Besides being a quite common targeting strategy, surface modification of NPs with functional motifs represents a unique tool to impart synergistic effects.[2] In the context of cancer, angiogenesis is an

orchestrated process crucial for the growth, invasion, and metastasis of a primary tumor.[19] The concept that disfunctional vasculature is common to a wide range of solid cancers has pushed the interest in tumor vascular targeting.[20, 21] Furthermore, stromal cells, unlike neoplastic cells, are genetically more stable, being less prone to develop resistance to therapy.[22] VEGF is the most relevant player in tumor angiogenesis, since its inhibition influence endothelial cell survival/growth/migration, blood flow, and stromal cell recruitment.[23] Anti-angiogenic therapy in cancer has nowadays reached maturity and distinct types of angiogenic inhibitors, such as antibodies and small molecules, have been introduced in the clinic (bevacizumab, tyrosine kinase inhibitors) to potentiate the response to chemotherapy, patient outcome, and survival in different cancer types.[24] However, non-selective anti-angiogenic therapies requires repeated i.v. administration[25] and may lead to worse response in terms of drug resistance, invasion, and metastasis.[26] To address the urgent need for new nano-oriented approaches in anti-angiogenic therapies[27], we have recently built up NPs of PEG-poly(ε-caprolactone) (PEG-PCL) surface-modified with the anti-angiogenic anti-FLT1 hexapeptide (aFLT1, GNQWFI), which selectively binds VEGFR1 isoform expressed in tumor dysfunctional capillaries.[28, 29] We found that NPs decorated with aFLT1 were superior to free aFLT1 in inhibiting tube vessel formation *in vitro* and potentiated the anticancer activity of docetaxel (DTX) in chicken embryo chorioallantoic membranes (CAM) xenografted with human triple-negative breast cancer cells.[30]

Based on these premises, here we propose an improved multifunctional therapeutic NP for the delivery of DTX which combines aFLT1 anti-angiogenic activity with Fol targeting. NPs, carrying the therapeutic cargo DTX in the core, are prepared from PEG-PCL copolymers conjugated with Fol and aFLT1 at PEG-OH end group and. After an in-depth characterization of NPs, their biological profile was tested in 2D and 3D cultures of FRα over-expressing KB human cervical cancer cells and in zebrafish embryos xenografted with the same type of cells.

2. Materials and Methods

2.1 Materials

mPEG-PCL (mPEG of 1.0 kDa, mPEG-PCL Mn 5.4 kDa), Fol-PEG-PCL (mPEG of 1.0 kDa, PCL Mn 4.7 kDa) and aFLT1-PEG-PCL (mPEG of 1.0 kDa, PCL Mn 4.7 kDa) were synthesized and characterized according to the procedures reported in our previous studies.[17, 31] Docetaxel (DTX) was purchased from LC laboratories (USA). 3,3′-dioctadecyloxacarbocyanine perchlorate (DiO) was purchased from ThermoFisher Scientific (Italy). Sodium chloride, potassium phosphate dibasic and potassium phosphate monobasic, sodium azide, and potassium chloride were used as received from Sigma Aldrich. All other solvents and chemicals were purchased from Sigma Aldrich (Milan, Italy) and used as received.

2.2 Preparation of NPs

We prepared bare PEGylated NPs (DBL) from mPEG-PCL copolymer, folate-targeted NPs (DBL_{Fol}) from mPEG-PCL/Fol-PEG-PCL (8:2 by weight, respectively), and antiangiogenic folated-targeted NPs ($DBL_{Fol/aFLT1}$) from mPEG-PCL/Fol-PEG-PCL/aFLT1-PEG-PCL (7:2:1 by weight, respectively). NPs were obtained by solvent diffusion of an organic phase (10 mg of copolymer/s in 1 mL of acetone) added dropwise in water (2 mL) under magnetic stirring (500 rpm). The addition of a surfactant was not required. After solvent evaporation, NPs were filtered through 0.45 μm Phenex® filters (Phenomenex, USA). NPs loaded with DTX were prepared according to the procedure reported above by adding DTX (1 mg) in acetone. Fluorescent NPs loaded with DiO were prepared with the same method by adding DiO (0.1 mg) in the organic phase.

2.3 NPs characterization

The hydrodynamic diameter (D_H), polydispersity index (PI), and zeta potential (ξ) of NPs were determined on a Zetasizer Nano ZS (Malvern Instruments Ltd). Results are reported as the mean of

three separate measurements of three different batches ± SD (n = 9). The yield of the NPs production process was evaluated on an aliquot of NPs dispersion by weighting the solid residue after freeze-drying. Results are expressed as the ratio of the actual NPs weight to the theoretical polymer or polymer + drug weight × 100 ± SD (n = 3).

DTX loading inside NPs was assessed by placing NPs (1 mg) in 500 μL of acetonitrile under stirring and then adding 500 μL of water. After that, the sample was filtered through a 0.45 μm filter (RC, Chemtek, Italy) and analysed to evaluate the DTX amount according to a previously reported HPLC method.[32] Briefly, the analysis was carried out on a Shimadzu apparatus (Japan) on a Juppiter 5 μm, C18 column. The mobile phase was a 55:45 (v/v) mixture of 0.1% TFA in water and acetonitrile pumped at a flow rate of 1 mL min^{-1}. The UV detector was set at 227 nm. A calibration curve for DTX in ethanol was plotted in the concentration range of 2–200 μg mL^{-1}. The release of DTX was determined on NPs (0.5 mg) dispersed in 0.5 mL of 10 mM phosphate buffer containing NaCl (137 mM) and KCl (2.7 mM) at pH 7.4 (PBS) at 37 °C and placed in a dialysis bag. The external phase (5 mL) was PBS again. At predetermined times, 1 mL aliquots of the sample were collected and then analyzed by HPLC.

Fixed aqueous layer thickness (FALT) of NPs was measured by monitoring the influence of ionic strength on ξ. Different amounts of NaCl stock solutions were added to NPs dispersed in water (250 μg/ mL) and zeta potential of the samples measured. A plot of ln ξ against $3.33*[NaCl]^{0.5}$ gives a straight line where the slope represents the thickness of the shell in nm.[33]

To evaluate the stability of NPs under physiologically relevant conditions, a known amount of NPs (1 mg) was diluted in PBS at pH 7.4 (NPs concentration 1 mg/mL) and incubated at 37 °C for different times. Size measurements of the samples were taken after 15 min, 1 h, 2 h, and 24 h of incubation as described above.

2.4 Dosage of folate exposure

Detection of folate on the NP surface was accomplished by incubating NPs with a specific mAB-antiFol (Monoclonal Anti-Folic Acid antibody produced in mouse, Sigma Aldrich) and determining its amount using the Bradford Assay. Briefly, 0.1 mL of NPs (5 mg/mL) were mixed with 0.1 mL of mAB-antiFol solution (34 μg/mL) in 10 mM PBS at pH 7.4, and the resulting solutions incubated for 1 h under mild shaking. The samples were then washed twice with PBS to remove the excess of antibody after centrifugation at 270000 x *g* for 20 min and finally re-dispersed in 0.5 mL of PBS followed by the addition of 500 μL of Bradford reagent. The resultant solutions were heated at 60 °C for 30 min and analyzed by UV spectrophotometry at 595 nm (Shimadzu UV 1800) according to the manufacturer's instructions. Using a calibration curve of free mAB-antiFol in PBS, the percentage of mAB bound to NP surface was determined. Each assay was repeated 3 times (each with n= 3 samples) and the average value was taken as the representative.

2.5 Generation of spheroids and NPs penetration

Multicellular spheroids of KB cells (ATCC, USA) were generated using the liquid overlay method, as previously reported.[34] After 3 days of growth, the spheroids had reached a diameter of about 500 μm and were used for the following experiments.

Three-days old KB spheroids were treated for 48 h with 50 μg/mL of DiO-loaded NPs. The localization/penetration of NPs was evaluated by confocal microscopy (Leica SP5) by transferring the spheroids from 96-well plates to 35 mm cell imaging dishes and washing them twice with PBS before visualization. Images of about 20 different focal planes (z-stack 10 μm) were acquired from the top to the bottom of the spheroid using a 10X objective. DiO fluorescence was revealed using a 488 nm laser as the excitation source and emission filters set from 505 to 550 nm. Maximum projection images were obtained with the software LAS AF Lite by superimposing the images of the

20 acquired focal planes. Furthermore, a 3D reconstruction of the distribution of the fluorescence signal in the equatorial plane of spheroids was obtained using the software ImageJ.

2.6 Cytotoxicity in spheroids

For cytotoxicity, spheroids were incubated for 48 or 72 h with 100 µL of fresh medium containing 10 % FBS and increasing concentration of free DTX or DTX-loaded NPs. At the end of incubation times, cell viability was measured using the CellTiter-Glo® 3D Cell Viability Assay (Promega), as previously reported.[35] During the experiment, the spheroid morphological changes were monitored with a bright-field microscope (DMI6000B, Leica) equipped with a DCF365FX camera.

2.7 Zebrafish handling and xenotransplantation

Experiments were performed at the Zebrafish Facility of the University of Padova, under ethical authorization 407/2015-PR. Embryos were obtained from natural spawning of *Casper* mutants (a9-w2 double mutant line; ZFIN IDs: ZDB-ALT-980203-444, ZDB-ALT-990423-22) and *fli1a:EGFP* transgenic adults (ZFIN ID: ZDB-ALT-011017-8), raised according to standard protocols [36] and staged according to Kimmel et al. [37] For xenotransplantation, embryos were mechanically dechorionated at 2 days post-fertilization (dpf), anesthetized with 0.16 mg/mL tricaine, and placed along the lanes of a microinjection mold, immersed in 2% methylcellulose/fish-water. KB cells were suspended at a density of 1×10^6/mL and stained with 5 µg/mL of DiI Vybrant Cell-Labeling Solution (Molecular Probes) for 20 min at 37 °C. Stained cells were loaded into a glass capillary needle and microinjected into the yolk (about 100 cells/embryo), using a WPI PicoPump apparatus. Twenty-four h after tumor transplantation (3 dpf), embryos were microinjected using the same procedures described above with an aqueous solution of phenol red (control), free DTX, DTX-loaded NPs (DTX-DBL, DBL_{Fol}, $DBL_{Fol/aFLT1}$) and unloaded $DBL_{Fol/aFLT1}$. Each embryo was injected with a DTX dose of about 2.5 ng; each experimental group of treatment was constituted of 25 embryos.

Xenotransplanted embryos were grown at 33 °C and monitored daily starting from the injection day up to 1-week post-injection (experimental endpoint, 9 dpf). Non-xenografted embryos injected with DTX formulations were observed in parallel. Analyses included mortality rate, *in situ* (yolk) or metastatic (extra yolk) cancer cell location, and tumor size reduction evaluation, performed by cell counting/signal quantification using ImageJ software. Imaging was performed using a Leica MZFLIII fluorescence-dissecting microscope equipped with a Leica DFC7000T camera.

For the analysis of neo-angiogenesis, the *fli1a:EGFP* transgenic line, having blood vessels and micro-vessels visible in green fluorescence, was used. The embryos (2 dpf) were injected with KB cells and 1 h later with DTX or DTX-$DBL_{Fol/aFLT1}$. Tumor and blood vessels were analysed 48 h later by fluorescence microscopy.

2.8 Statistical analysis

The Primer software for biostatistics (McGraw-Hill, Columbus, USA) was used for statistical analysis of the data. The data are expressed as means ± standard deviations (SD) for at least 3 independent experiments. The difference between groups was evaluated with the Student's t-test and was considered significant for $p < 0.05$.

3. Results and discussion

3.1 NPs preparation and characterization

In this work we conceived a multifunctional NP for cancer therapy applications, in which the active targeting of the therapeutic cargo is complemented with anti-angiogenic effects. Accordingly, we designed a NP delivering DTX based on a mix of PCL-PEG copolymers, some of which modified at the PEG end chain with either aFLT1 or Fol to obtain the multifunctional nanoplatform with double decoration ($DBL_{Fol/aFLT1}$) (Fig 1A). For comparison purposes, unmodified NPs of PEG-PCL (DBL), aFLT1-PEG-PCL/PEG-PCL (DBL_{aFLT1}), or Fol-PEG-PCL/PEG-PCL (DBL_{Fol}) were prepared.

Unloaded or DTX-loaded NPs were obtained by the solvent diffusion/evaporation method. The ratio between Fol-PEG-PCL/PEG-PCL and Fol-PEG-PCL/aFLT1-PEG-PCL was selected based on our previous findings[17, 30]. It is worth noting that the manipulation space in this sense was limited due to aggregation of the sample in the nanoprecipitation step when Fol-PEG-PCL or aFLT1-PEG-PCL amount was increased and that of PEG-PCL was decreased. The overall properties of the NPs are reported in Table 1.

Table 1. Properties of unloaded and DTX-loaded NPs

Formulation	D_H (nm ± SD)	PI	ζ (mV ± SD)	Yield (%± SD)	DTX Actual loading (mg DTX/100 mg NPs)	DTX Entrapment Eff.[a] (%)
DBL	78 ± 2	0.1	-12 ± 0.1	68 ± 4	-	-
DBL_{Fol}	84 ± 5	0.1	-18 ± 6	52 ± 3	-	-
$DBL_{Fol/aFLT1}$	101 ± 8	0.2	-10 ± 3	54 ± 1	-	-
DTX-DBL	92 ± 5	0.2	-10 ± 1	72 ± 6	8.8 ± 0.9	98 ± 4
DTX-DBL_{Fol}	84 ± 8	0.1	-19 ± 4	61 ± 4	8.7 ± 1.5	98 ± 10
DTX-$DBL_{Fol/aFLT1}$	101 ± 5	0.1	-9 ± 2	55 ± 3	8.5 ± 0.6	96 ± 6

[a] Theoretical loading of DTX was 9 mg DTX *per* 100 mg of NPs.

All the formulations show a D_H between 78 and 101 nm, a low polydispersity index, and a negative ζ. NPs prepared from copolymer mix (DBL_{Fol} and $DBL_{Fol/aFLT1}$) are larger as compared with DBL, suggesting that a segregation of hydrophilic blocks in the PCL core occurs[17].

In Figure 1B, the values of ξ in NaCl solutions at different concentrations are shown. The thickness of the external hydrophilic PEG shell of NPs, which is the slope of the regression lines in absolute value, is similar for the NPs tested, thus suggesting that the presence of surface motifs has a slight impact on the conformation of the PEG present on the surface of NPs (Fig. 1B). DTX entrapment in in the lipophilic core of NPs (9% theoretical loading) is almost complete and does not affect colloidal properties of NPs.

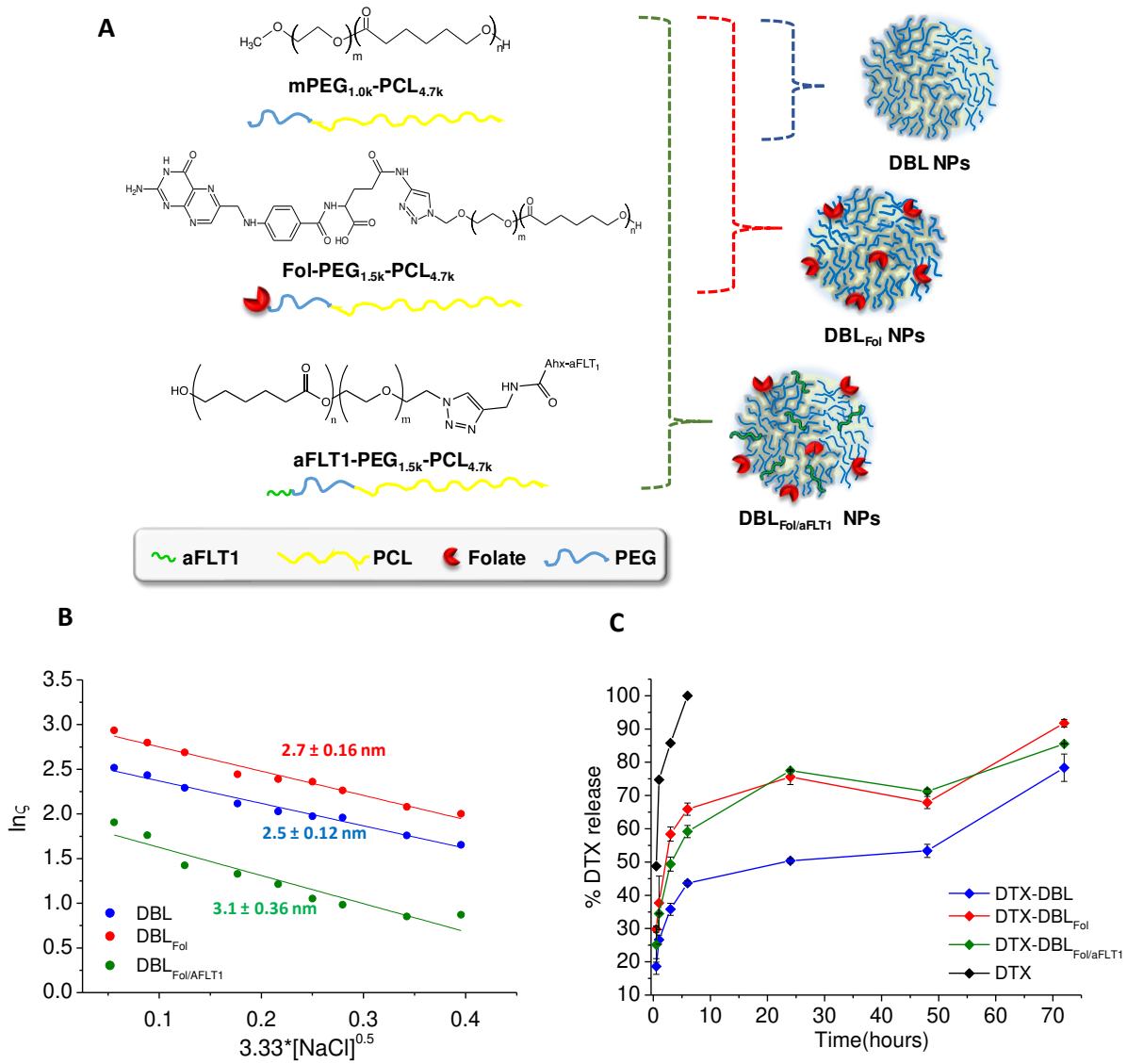

Figure 1. A) NPs composition; B) Representative FALT measurements: the slope of the straight line represents the thickness of the outer hydrophilic shell expressed in nm; C) DTX release from NPs in PBS 10 mM pH 7.4, at 37 °C evaluated by the dialysis method. Results are the mean values ± SD of three measurements carried out on three different NPs batches.

The release of DTX from NPs (Fig. 1C), evaluated in 10 mM PBS at pH 7.4 and 37 °C by dialysis, is bimodal for all the formulations. The burst in the 0-6 h interval is higher for NPs obtained from copolymer mix as compared to bare DBL, in line with the hypothesis that the presence of some hydrophilic blocks in the PCL core matrix decrease the crystallinity of the NP core and increase diffusivity of the entrapped DTX. Release of DTX is completed in ca. 72 h for all the formulations

tested. Free DTX is quantitatively released in the external medium in ca. 6 h, which ensures the occurrence of sink conditions.

As shown in Fig. 2A, NPs show excellent stability in PBS pH 7.4 at 37 °C, employed as simulated biological studies until 24 h of incubation. Then, the exposure of folate on NP surface was checked through the binding with a specific mAB against folate. As evident in Fig. 2B, the 40% of antibody was able to bind DBL_{Fol} and $DBL_{Fol/aFLT1}$ NPs, independently by the presence of the antiangiogenic peptide. The experiment was carried out also on untargeted NPs as negative control.

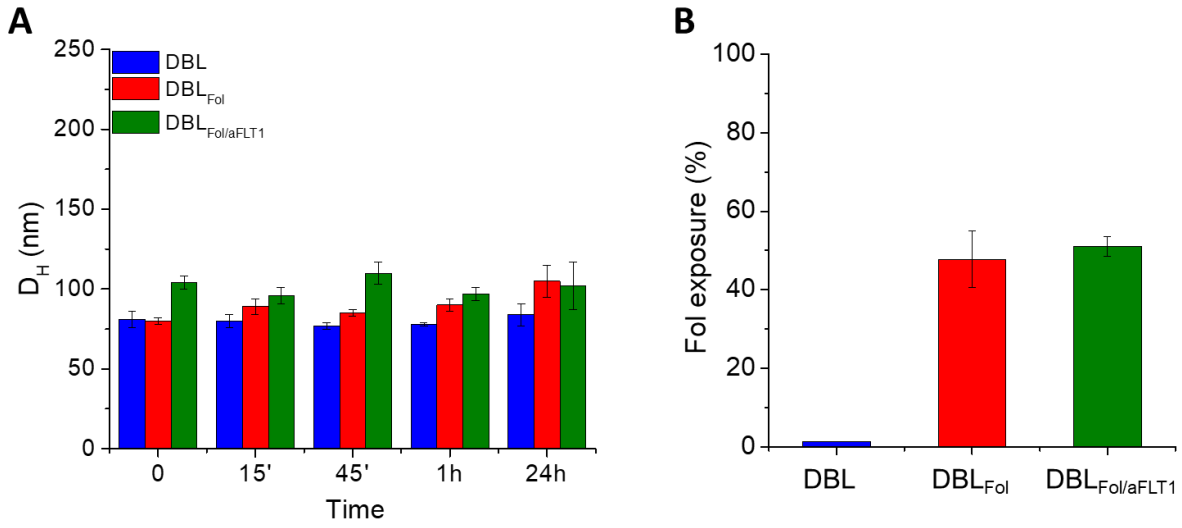

Figure 2. A) D_H of NPs after incubation in PBS pH 7.4 at 37 °C; B) Exposure of folate moieties on nanoparticle surface. Results are the mean values ± SD of three measurements carried out on three different NPs batches.

Then, before moving to *in vitro* and *in vivo* experimentation, we checked NPs interaction with proteins present in simulated biological fluids. Thus, NPs were dispersed in RPMI cell culture medium added with 10% Fetal Bovine Serum (FBS) and the quenching of FBS emission after excitation at 278 nm was evaluated. We found a similar interaction between the proteins and the different formulations, slightly pronounced in the case of $DBL_{Fol/aFLT1}$ NPs and DBL_{Fol} (Fig. S1). Finally, we confirmed the elevated antiangiogenic activity of aFLT1 displayed on the surface of

$DBL_{Fol/aFLT1}$: compared with DBL and DBL_{Fol} which, has expected, did not show any capacity to inhibit endothelial tube formation (Fig. S2), $DBL_{Fol/aFLT1}$ significantly affect all tube parameters (e.g. number of junctions, master segments and meshes).

3.2 In vitro behavior of NPs in KB spheroids

The behaviour of DTX-loaded NPs was assessed in FRα positive KB cells cultured as avascular spheroids to mimic more closely the *in vivo* three-dimensional tumor architecture and the enrichment in extracellular matrix components, which may affect drug distribution and efficacy.[38] The penetration of DBL_{Fol} and $DBL_{Fol/aFLT1}$ NPs loaded with DiO (properties in Table S1) in KB spheroids is shown in Fig. 3. Confocal images taken at the median plane of the spheroids after 48 h of incubation evidence a different distribution pattern depending on NP decoration. Due to the high lipophilicity of DiO, we assume that the green fluorescence visible in the cell aggregates can be identified with NPs. While fluorescence is randomly distributed for DBL, green signal is confined in the outer rims for DBL_{Fol} and uniformly distributed in the entire spheroid for $DBL_{Fol/aFLT1}$. Tridimensional plots showing fluorescence signal intensity (Fig 4, panels c) and maximum projections (Fig. 4, panels d) revealed that NPs accumulated in the order DBL < $DBL_{Fol/aFLT1}$ <DBL_{Fol} as compared to the total fluorescence. The prevalent location of DBL_{Fol} in the spheroid rim is in line with the so-called "barrier effect" observed for NPs targeting cancer cells receptors. Surprisingly, the parallel presence of aFLT1 on NP surface attenuates this effect and promotes $DBL_{Fol/aFLT1}$ penetration in the whole cell aggregate, likely due to a shielding effect exerted by peptide chains.

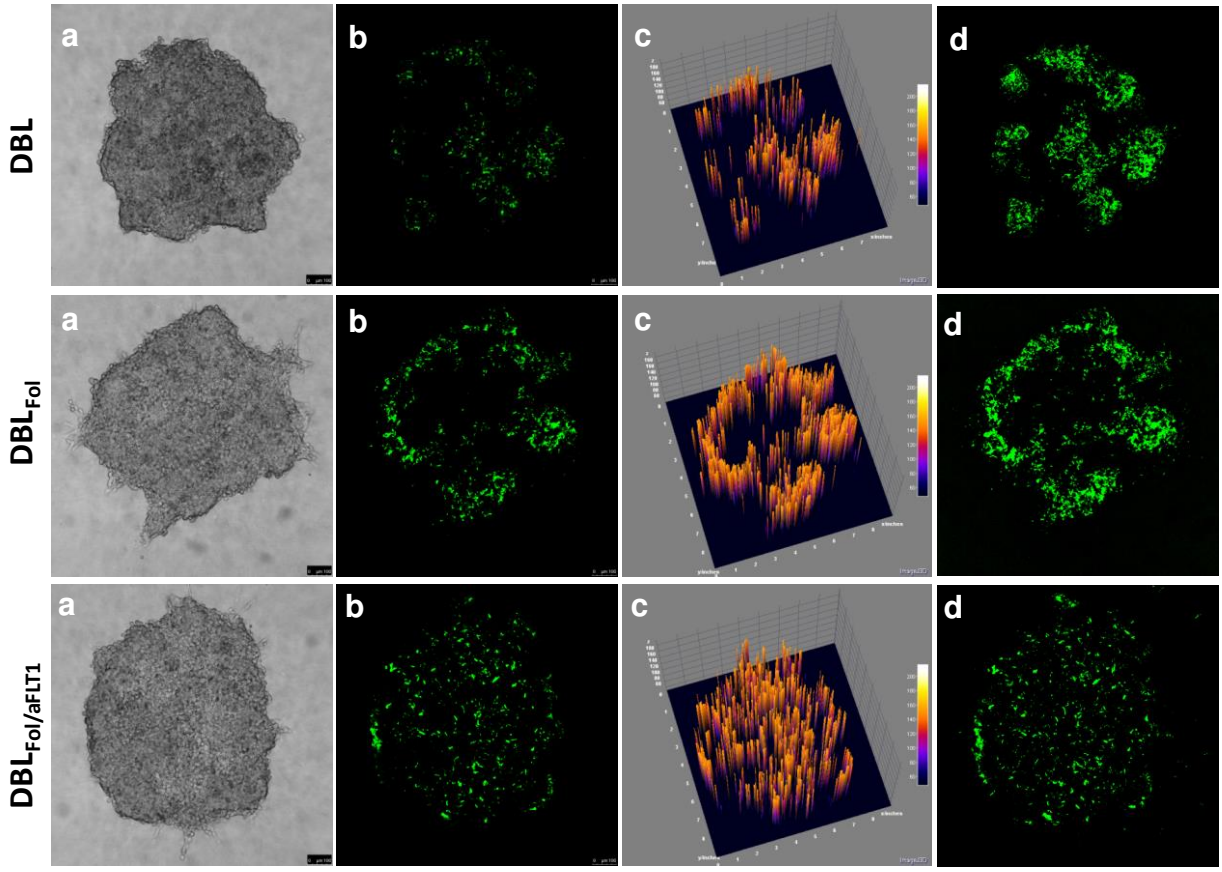

Figure 3. Confocal images of KB spheroids after treatment with DiO-loaded NPs (50 µg/mL) for 48 h: a) bright-field; b) DiO fluorescence acquired in the equatorial plane of the spheroid c) 3D reconstruction of the distribution of the fluorescence signal in the equatorial plane of the spheroid; d) maximum projection. Scale bars: 100 µm.

A concentration- and time-dependent cell viability reduction was measured upon treatment of 2D cultures of both KB and HUVEC with DTX and DTX-loaded NPs (Fig. S3). Cell viability of DTX-DBL$_{Fol}$ and DTX-DBL$_{Fol/aFLT1}$ vs. DTX-DBL was not modified by surface decoration, probably due to the weak contribution of FR-mediated NPs endocytosis as compared to non-specific endocytosis, as we previously reported for monolayer cell cultures,[17] maybe also due to interaction with proteins in the cell media thus shielding folate exposition.

The cytotoxicity of DTX-loaded NPs measured by the 3D Glo Assay in KB spheroids after 72 h of treatment is reported in Fig. 4. Results are expressed as residual ATP content *vs.* untreated cells as a significant parameter to measure viability reduction and toxicity. The incubation of KB spheroids

with DTX-loaded NPs determines a sharp cell viability reduction, although no significant differences between the formulations were observed independently of the time (see also Fig. S4 reporting cell viability of spheroid after 48 h of incubation). The cytotoxicity of free DTX is dose- and time-dependent as well as confirmed by the bright-field images of the treated spheroids (Fig. 4B and Fig. S4B) highlighting that the progressive loss of viability is accompanied by the disaggregation of cells constituting the spheroids. As expected, the extent of cell release and mortality started from the periphery to the core of the spheroids, especially with DTX-DBL$_{Fol}$ and DTX-DBL$_{Fol/aFLT1}$ at a drug concentration of 0.01 μg/mL for both 48 and 72 h. Unloaded NPs were not toxic to cell spheroids (Fig. S5).

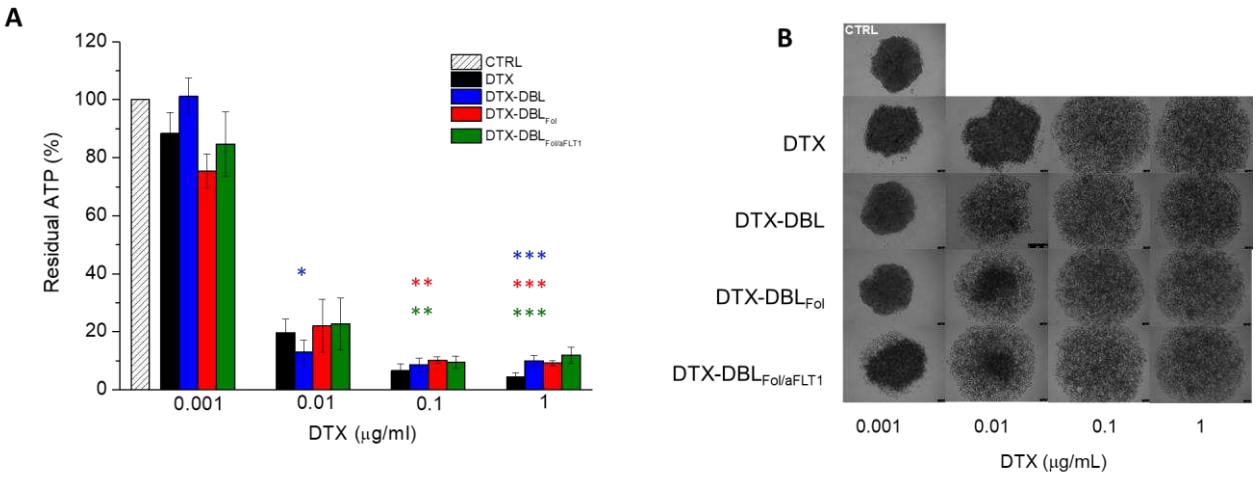

Figure 4. Cytotoxicity of DTX-loaded NPs in KB spheroids: A) Residual ATP after 72 h of treatment. Data are mean values ± SD of at least three independent experiments carried out in triplicate. *p<0.05, **p<0.01, ***p<0.001 *vs* free DTX (*Student's t-test*); B) Bright-field images of spheroids after 72 h of treatment with DTX-loaded NPs at different doses. Scale bars: 100 μm.

The different pattern of cellular aggregate dissociation is consistent with the observation that the presence of Fol decoration of NPs promoted the accumulation mainly at the periphery of the spheroid and exert cytotoxic effects prevalently in the rim. The fact that cytotoxicity of NPs is comparable

with that of DTX demonstrate once again that a complex interplay between DTX release and NP transport/accumulation in the cancer cell aggregates occur, making difficult to draw final conclusions on superior activity of NPs.

3.4 In vivo anti-tumor and anti-angiogenic activity of NPs in zebrafish embryos

The choice of using *Danio rerio* embryos as an exploratory *in vivo* model to study tumor regression and angiogenesis after treatment with NPs was encouraged by several preliminary considerations,[39]: i) the transparency of the embryo, which allows easy observation of tumor development, angiogenesis, and metastasis in real-time; ii) high physiologic and genetic similarity to mammals,[39]; iii) low cost of maintenance and ease of manipulation as compared to rodents. Furthermore, the immune system of embryos is immature up to 11 dpf, thus avoiding or delaying the rejection of xenotransplants.[40] The availability of transgenic models over-expressing fluorescent proteins (e.g., vascular proteins) also offers a tool to easily monitor neo-angiogenesis.[41, 42]

The set-up of the experiments in albino zebrafish embryos xenografted with KB cells is outlined in Figure 5A. The yolk region of 2 dpf embryos was inoculated with DiI-labeled KB cells, and the following day re-injected with DTX, DTX-loaded NPs as well as with unloaded DBL as control. At the time of NP inoculation, KB cells are confined in the yolk of the embryos forming a single mass with spherical shape and a mean diameter of about 600-800 μm, a size close to that of spheroids tested *in vitro* (Fig. 5A).

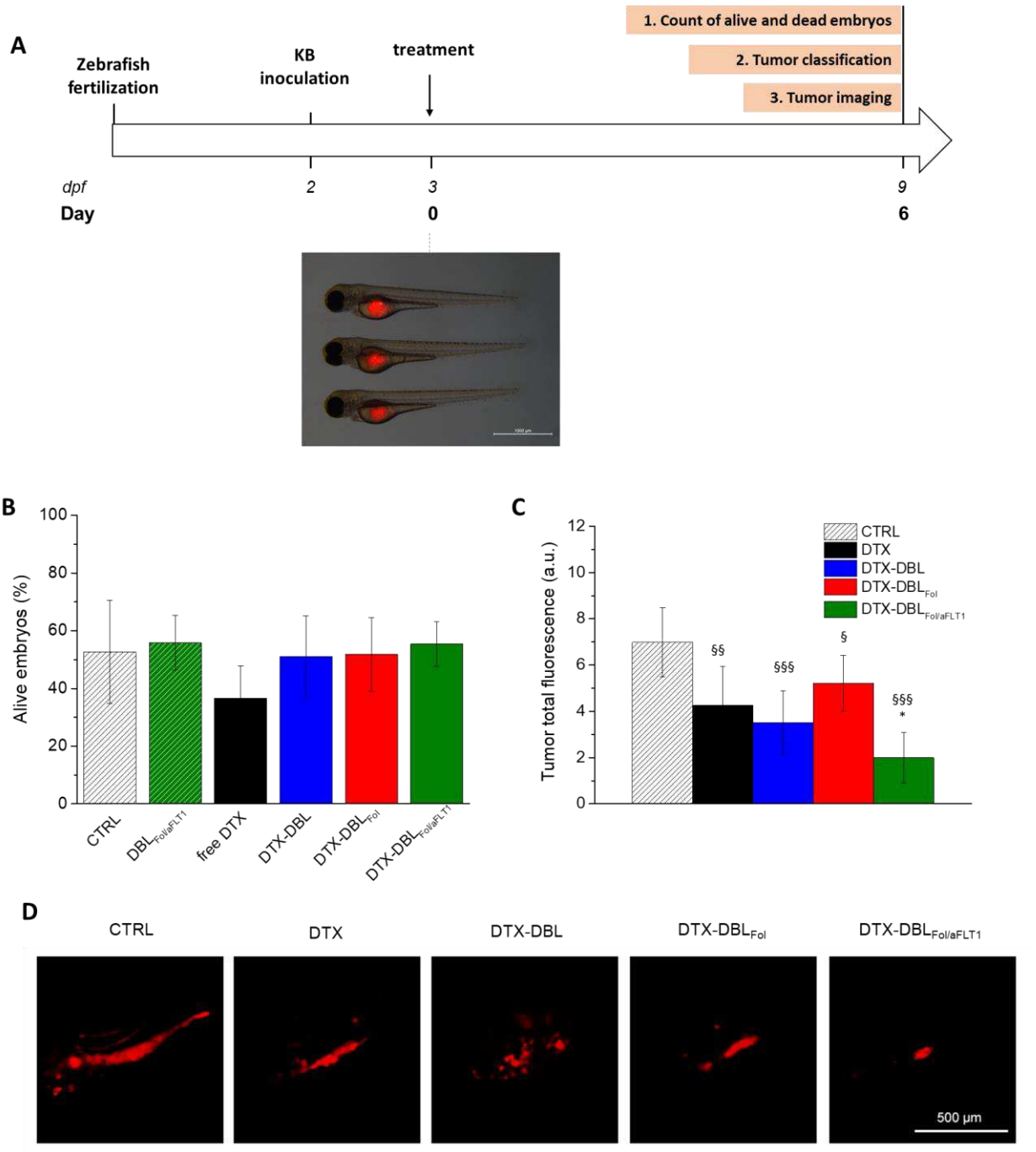

Figure 5. Toxicity and activity of DTX-loaded NPs in the zebrafish embryo xenograft model. A) Timeline of the *in vivo* experiments. The microscopy image shows 3 embryos xenografted with KB cells (red fluorescence). B) Toxicity of NPs in xenograft zebrafish embryos injected with DTX and DTX-loaded NPs ([DTX]= 2.5 ng/animal) after 6 days from the treatment. C) Tumor volume reduction after 6 days from the treatment. Total tumor fluorescence quantified from images. § $p < 0.05$; §§ $p < 0.01$; §§§ $p < 0.001$ *vs.* ctrl; * $p<0.001$ *vs* free DTX. D) Representative images of KB cells xenotransplanted in the embryo yolks. Scale bars 500 µm.

Animal survival analysis revealed that, in the case of embryos xenografted with KB cells, the percentages of alive animals decreased to 50% for the control group and all the variants of DTX-loaded NPs (Fig. 5C) as compared with 70% for the same groups in non-xenografted animals (Fig. S6). Remarkably, DTX treatment reduced the percentage of alive embryos from 70 % to 40% in the non-xenograft embryos (Fig. S6), thus highlighting the role of NPs in protecting the embryo from the high systemic toxicity of DTX.

The efficacy of DTX-loaded NPs in reducing effectively tumor masses was assessed on selected animals bearing a single mass in the yolk 6-days post-treatment. As clearly visible in Fig. 5C, a high reduction of KB-associated fluorescence in all the treated groups compared to control was observed. Notably, the greatest extent of tumor reduction was obtained with DTX-DBL$_{Fol/aFLT1}$, which means that an improvement of DTX efficacy takes place due to the presence of both the targeting and the anti-angiogenic motifs. Noteworthy, the presence of Fol on NPs surface did not result in any tumor size reduction improvement as compared to untargeted NPs. In fact, three different tumor conditions (indicated as tumor phenotypes) occurred after 6 days of treatment as exemplified with representative images in Figure S7A: single masses located in the yolk (a), multiple masses located in the yolk (b), tumor masses in the yolk plus distal masses (metastasis-like masses) outside yolk region (c). Cell migration from the yolk region is considered indicative of cell invasiveness.[43] The percentages of tumor phenotypes are reported in Fig. S7B. Overall, the extent of cell invasiveness was quite low (~20%), and only DTX-DBL$_{Fol}$ significantly reduced KB cell spread. Moreover, while in the control group, the number of animals with single or multiple masses in the yolk was comparable, the treatment with free DTX and DTX-DBL$_{Fol/aFLT1}$ completely abolished the formation of multiple tumor masses, with about 70% of alive embryos having a single tumor mass. Differently from the *in vitro* observations, tumor regression observed in zebrafish highlighted the superior activity of DTX-DBL$_{Fol/aFLT1}$ as compared to free DTX accompanied by a concomitant decrease of DTX systemic toxicity.

To understand if this effect was related to the anti-angiogenic activity of DTX-DBL$_{Fol/aFLT1}$, we employed a *fli1a:EGFP* transgenic embryo model. We analysed eventual macroscopic alterations of blood vessel features 48 h after NPs injection and compared the results to those collected from untreated or DTX-treated embryos. Fig. 6A and 6B are representative images of a embryo (untreated) xenografted or not with KB cells, respectively. In both embryos, the intact sub-intestinal vessels (SIVs), with a shape like a basket projected inside the yolk region, are completely formed at this development stage. As clearly visible in Fig. 6, panel B1, and according to some recent pieces of evidence [44], the injection of tumor cells induces pro-angiogenic effects by promoting the formation of additional branches (white circles), which essentially sprout toward the tumor mass.

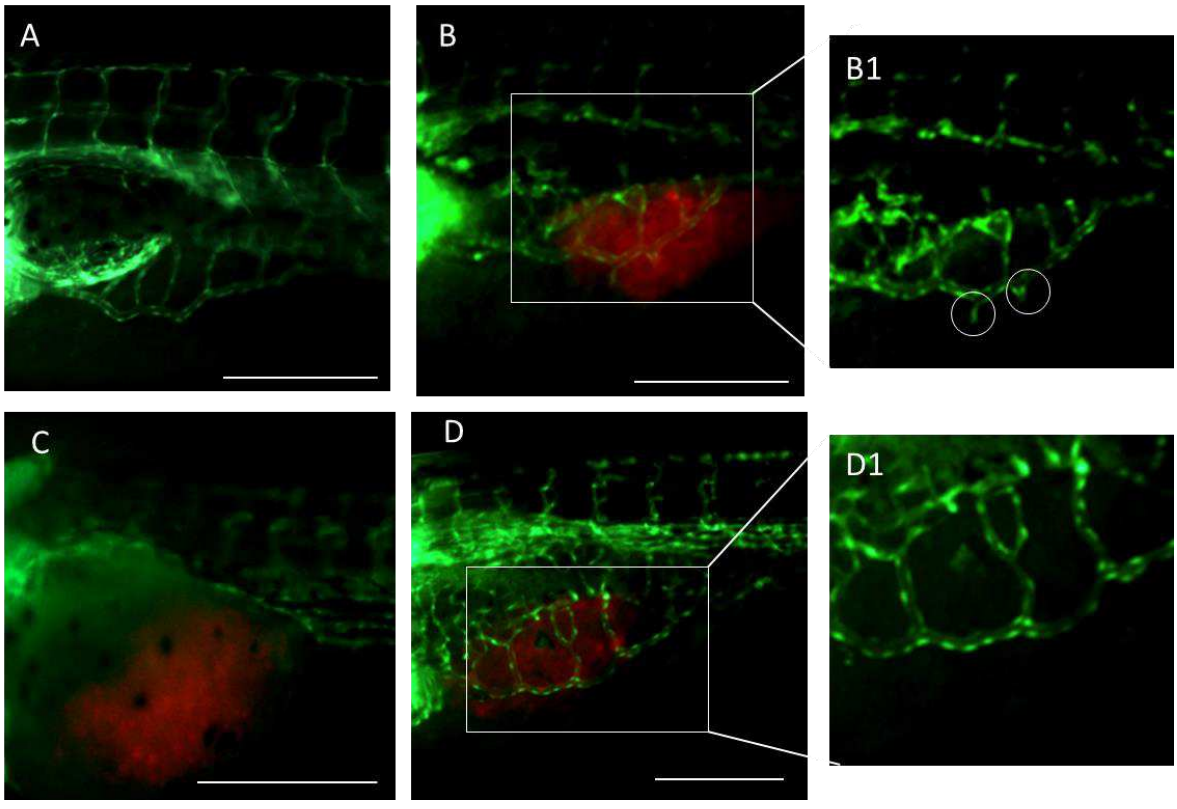

Figure 6. Vasculature analysis of *fli1a:EGFP* embryos after two days of NPs treatment. Fluorescence microscopy images of untreated embryos without (A) or with KB xenografted cells (B); embryos with KB xenografted cells and treated with free DTX (C) or DTX-DBL$_{Fol/aFLT1}$ (D). B1 is a magnification showing the presence of vascular branches (white circles) sprouting toward tumor masses in untreated embryos. In the magnification D1 vascular branches are not visible due to the

anti-angiogenic effect exerted by DTX-DBL$_{Fol/aFLT1}$. Scale bar 250 μm. Red: tumor cells stained with DiI; green: zebrafish embryo vasculature.

Interestingly, the treatment of the xenografted embryos with DTX-DBL$_{Fol/aFLT1}$ prevented the formation of these branches (Fig. 6D, D1), thus suggesting an active role of aFLT1. After DTX treatment the classic basket structure was not formed (Fig. 6C) and the vessels were utterly disorganized within the swollen yolk sack, which is in line with its superior systemic toxicity.

Taken together, our results demonstrate that tumor regression due to DTX-DBL$_{Fol/aFLT1}$ is due to DTX cytotoxicity combined with a significant anti-angiogenic capacity of NPs, which normalize vessels rather than completely disrupt endothelial cells. Importantly, while we were unable to measure any active role of the folate moiety in the *in vitro* model, DTX-DBL$_{Fol}$ NPs attenuated overall toxicity of DTX and demonstrated both an increased anticancer effect and a decreased spread of metastasis in the xenografted zebrafish. The latter observation stresses the importance of the *in vivo* studies to test NPs efficacy, even using experimental models alternative to rodents as zebrafish, and highlight that also three-dimensional *in vitro* models as spheroids, are by themselves only poorly predictive of *in vivo* behaviour.

Conclusion

We have herein reported the development of PEGylated NPs surface-modified with folate/aFLT1 motifs as a strategy to potentiate the activity profile of DTX and to limit its systemic toxicity. The presence of folate on NP surface did not alter aFLT1 anti-angiogenic activity, whereas affected their penetration in KB spheroids. No significant impact of NP composition on cytotoxicity in the spheroids was found. Remarkably, DTX activity was enhanced in a xenografted zebrafish embryo model when delivered through NPs bearing folate/aFLT1 motifs, whereas DTX toxicity was decreased. To our knowledge, this is the first demonstration that such double decoration of biodegradable PEGylated NPs is feasible and useful to increase the efficacy of the bare PEGylated

counterpart. Our findings can pave the way to the extension of this NP concept to other anti-angiogenic peptides and chemotherapeutics, widening the arsenal of nanoplatforms to fight solid tumors.

ETHICAL STATEMENT

Ethics approval and consent to participate:

Not applicable

Consent for publication:

All authors have seen and approved the text presented data in this work.

Availability of data and materials:

The raw data are available from the authors.

Competing interests:

The authors declare no competing interests.

Authors' contributions:

F. M. performed the biological studies on cells and contributed to manuscript draft; C.C. performed the studies on nanoparticles and contributed to manuscript draft; D.E. manufactured and characterized the samples; G.D.P synthesized the polymers; C.A. synthesized the peptides; F.U. supervised the characterization studies; N.T. performed the biological studies on zebrafish; A.R. supervised peptide synthetic procedures; P.L.supervised polymer synthetic procedures and drafted the manuscript; E.R. supervised biological study; F.Q.coordinated the research, analyzed the results and wrote the manuscript.

Acknowledgments and Funding:

This work was supported by the Italian Association for Cancer Research (IG2014 n.15764), the Regione Campania-POR Campania FESR 2014/2020 “Combattere la resistenza tumorale:

piattaforma integrata multidisciplinare per un approccio tecnologico innovativo alle oncoterapie-Campania Oncoterapie" (Project N. B61G18000470007) and the Department of Biology, University of Padova (PRIDseed 2018 Grant to FM).

Supplementary materials

See corresponding file.

References

1. Kydd, J.; Jadia, R.; Velpurisiva, P.; Gad, A.; Paliwal, S.; Rai, P., Targeting Strategies for the Combination Treatment of Cancer Using Drug Delivery Systems. Pharmaceutics 2017, 9 (4).
2. Seeta Rama Raju, G.; Benton, L.; Pavitra, E.; Yu, J. S., Multifunctional nanoparticles: recent progress in cancer therapeutics. Chemical communications 2015, 51 (68), 13248-59.
3. Karlsson, J.; Vaughan, H. J.; Green, J. J., Biodegradable Polymeric Nanoparticles for Therapeutic Cancer Treatments. Annu Rev Chem Biomol Eng 2018, 9, 105-127.
4. Kemp, J. A.; Shim, M. S.; Heo, C. Y.; Kwon, Y. J., "Combo" nanomedicine: Co-delivery of multi-modal therapeutics for efficient, targeted, and safe cancer therapy. Advanced drug delivery reviews 2016, 98, 3-18.
5. Hillmyer, M. A.; Tolman, W. B., Aliphatic Polyester Block Polymers: Renewable, Degradable, and Sustainable. Accounts of Chemical Research 2014, 47 (8), 2390-2396.
6. Tian, H.; Tang, Z.; Zhuang, X.; Chen, X.; Jing, X., Biodegradable synthetic polymers: Preparation, functionalization and biomedical application. Progress in Polymer Science 2012, 37 (2), 237-280.
7. d'Angelo, I.; Conte, C.; Miro, A.; Quaglia, F.; Ungaro, F., Core-shell nanocarriers for cancer therapy. Part I: biologically oriented design rules. Expert Opin Drug Deliv 2014, 11 (2), 283-97.
8. Owens, D. E.; Peppas, N. A., Opsonization, biodistribution, and pharmacokinetics of polymeric nanoparticles. International journal of pharmaceutics 2006, 307 (1), 93-102.
9. Suk, J. S.; Xu, Q.; Kim, N.; Hanes, J.; Ensign, L. M., PEGylation as a strategy for improving nanoparticle-based drug and gene delivery. Advanced drug delivery reviews 2016, 99 (Pt A), 28-51.
10. Alexis, F.; Pridgen, E.; Molnar, L. K.; Farokhzad, O. C., Factors Affecting the Clearance and Biodistribution of Polymeric Nanoparticles. Molecular Pharmaceutics 2008, 5 (4), 505-515.
11. Conte, C.; Dal Poggetto, G.; B, J. S.; Esposito, D.; Ungaro, F.; Laurienzo, P.; Boraschi, D.; Quaglia, F., Surface Exposure of PEG and Amines on Biodegradable Nanoparticles as a Strategy to Tune Their Interaction with Protein-Rich Biological Media. Nanomaterials (Basel) 2019, 9 (10).
12. Behzadi, S.; Serpooshan, V.; Tao, W.; Hamaly, M. A.; Alkawareek, M. Y.; Dreaden, E. C.; Brown, D.; Alkilany, A. M.; Farokhzad, O. C.; Mahmoudi, M., Cellular uptake of nanoparticles: journey inside the cell. Chemical Society Reviews 2017, 46 (14), 4218-4244.
13. Danhier, F.; Feron, O.; Preat, V., To exploit the tumor microenvironment: Passive and active tumor targeting of nanocarriers for anti-cancer drug delivery. Journal of controlled release : official journal of the Controlled Release Society 2010, 148 (2), 135-46.
14. Farran, B.; Montenegro, R. C.; Kasa, P.; Pavitra, E.; Huh, Y. S.; Han, Y.-K.; Kamal, M. A.; Nagaraju, G. P.; Rama Raju, G. S., Folate-conjugated nanovehicles: Strategies for cancer therapy. Materials Science and Engineering: C 2020, 107, 110341.

15. Valencia, P. M.; Hanewich-Hollatz, M. H.; Gao, W.; Karim, F.; Langer, R.; Karnik, R.; Farokhzad, O. C., Effects of ligands with different water solubilities on self-assembly and properties of targeted nanoparticles. Biomaterials 2011, 32 (26), 6226-6233.
16. Kularatne, S. A.; Low, P. S., Targeting of nanoparticles: folate receptor. Methods in molecular biology 2010, 624, 249-65.
17. Venuta, A.; Moret, F.; Dal Poggetto, G.; Esposito, D.; Fraix, A.; Avitabile, C.; Ungaro, F.; Malinconico, M.; Sortino, S.; Romanelli, A.; Laurienzo, P.; Reddi, E.; Quaglia, F., Shedding light on surface exposition of poly(ethylene glycol) and folate targeting units on nanoparticles of poly(epsilon-caprolactone) diblock copolymers: Beyond a paradigm. European journal of pharmaceutical sciences : official journal of the European Federation for Pharmaceutical Sciences 2018, 111, 177-185.
18. Conte, C.; Fotticchia, I.; Tirino, P.; Moret, F.; Pagano, B.; Gref, R.; Ungaro, F.; Reddi, E.; Giancola, C.; Quaglia, F., Cyclodextrin-assisted assembly of PEGylated polyester nanoparticles decorated with folate. Colloids Surf B Biointerfaces 2016, 141, 148-157.
19. Zuazo-Gaztelu, I.; Casanovas, O., Unraveling the Role of Angiogenesis in Cancer Ecosystems. Front Oncol 2018, 8, 248.
20. Atukorale, P. U.; Covarrubias, G.; Bauer, L.; Karathanasis, E., Vascular targeting of nanoparticles for molecular imaging of diseased endothelium. Advanced drug delivery reviews 2017, 113, 141-156.
21. Sakurai, Y.; Akita, H.; Harashima, H., Targeting Tumor Endothelial Cells with Nanoparticles. Int J Mol Sci 2019, 20 (23), 5819.
22. Valkenburg, K. C.; de Groot, A. E.; Pienta, K. J., Targeting the tumour stroma to improve cancer therapy. Nat Rev Clin Oncol 2018, 15 (6), 366-381.
23. Kamba, T.; McDonald, D. M., Mechanisms of adverse effects of anti-VEGF therapy for cancer. Br J Cancer 2007, 96 (12), 1788-95.
24. Vasudev, N. S.; Reynolds, A. R., Anti-angiogenic therapy for cancer: current progress, unresolved questions and future directions. Angiogenesis 2014, 17 (3), 471-494.
25. Benny, O.; Fainaru, O.; Adini, A.; Cassiola, F.; Bazinet, L.; Adini, I.; Pravda, E.; Nahmias, Y.; Koirala, S.; Corfas, G.; D'Amato, R. J.; Folkman, J., An orally delivered small-molecule formulation with antiangiogenic and anticancer activity. Nature biotechnology 2008, 26 (7), 799-807.
26. Ebos, J. M. L.; Lee, C. R.; Kerbel, R. S., Tumor and Host-Mediated Pathways of Resistance and Disease Progression in Response to Antiangiogenic Therapy. Clinical Cancer Research 2009, 15 (16), 5020-5025.
27. Kargozar, S.; Baino, F.; Hamzehlou, S.; Hamblin, M. R.; Mozafari, M., Nanotechnology for angiogenesis: opportunities and challenges. Chem Soc Rev 2020, 49 (14), 5008-5057.
28. Bae, D. G.; Kim, T. D.; Li, G.; Yoon, W. H.; Chae, C. B., Anti-flt1 peptide, a vascular endothelial growth factor receptor 1-specific hexapeptide, inhibits tumor growth and metastasis. Clinical cancer research : an official journal of the American Association for Cancer Research 2005, 11 (7), 2651-61.
29. Fischer, C.; Mazzone, M.; Jonckx, B.; Carmeliet, P., FLT1 and its ligands VEGFB and PlGF: drug targets for anti-angiogenic therapy? Nature reviews. Cancer 2008, 8 (12), 942-56.
30. Conte, C.; Moret, F.; Esposito, D.; Dal Poggetto, G.; Avitabile, C.; Ungaro, F.; Romanelli, A.; Laurienzo, P.; Reddi, E.; Quaglia, F., Biodegradable nanoparticles exposing a short anti-FLT1 peptide as antiangiogenic platform to complement docetaxel anticancer activity. Materials science & engineering. C, Materials for biological applications 2019, 102, 876-886.
31. Castelani, L.; Arcaro, J. R. P.; Braga, J. E. P.; Bosso, A. S.; Moura, Q.; Esposito, F.; Sauter, I. P.; Cortez, M.; Lincopan, N., Short communication: Activity of nisin, lipid bilayer fragments and cationic nisin-lipid nanoparticles against multidrug-resistant Staphylococcus spp. isolated from bovine mastitis. Journal of dairy science 2019, 102 (1), 678-683.

32. Palma, G.; Conte, C.; Barbieri, A.; Bimonte, S.; Luciano, A.; Rea, D.; Ungaro, F.; Tirino, P.; Quaglia, F.; Arra, C., Antitumor activity of PEGylated biodegradable nanoparticles for sustained release of docetaxel in triple-negative breast cancer. International journal of pharmaceutics 2014, 473 (1-2), 55-63.
33. Endres, T. K.; Beck-Broichsitter, M.; Samsonova, O.; Renette, T.; Kissel, T. H., Self-assembled biodegradable amphiphilic PEG-PCL-lPEI triblock copolymers at the borderline between micelles and nanoparticles designed for drug and gene delivery. Biomaterials 2011, 32 (30), 7721-31.
34. Gaio, E.; Scheglmann, D.; Reddi, E.; Moret, F., Uptake and photo-toxicity of Foscan(R), Foslip(R) and Fospeg(R) in multicellular tumor spheroids. Journal of photochemistry and photobiology. B, Biology 2016, 161, 244-52.
35. Gaio, E.; Guerrini, A.; Ballestri, M.; Varchi, G.; Ferroni, C.; Martella, E.; Columbaro, M.; Moret, F.; Reddi, E., Keratin nanoparticles co-delivering Docetaxel and Chlorin e6 promote synergic interaction between chemo- and photo-dynamic therapies. Journal of photochemistry and photobiology. B, Biology 2019, 199, 111598.
36. Westerfield, M., The zebrafish book. A guide for the laboratory use of zebrafish (Danio rerio). 4th ed ed.; Univ. of Oregon Press, Eugene.: 2000.
37. Kimmel, C. B.; Ballard, W. W.; Kimmel, S. R.; Ullmann, B.; Schilling, T. F., Stages of embryonic development of the zebrafish. Developmental dynamics : an official publication of the American Association of Anatomists 1995, 203 (3), 253-310.
38. Millard, M.; Yakavets, I.; Zorin, V.; Kulmukhamedova, A.; Marchal, S.; Bezdetnaya, L., Drug delivery to solid tumors: the predictive value of the multicellular tumor spheroid model for nanomedicine screening. International journal of nanomedicine 2017, 12, 7993-8007.
39. Barros, T. P.; Alderton, W. K.; Reynolds, H. M.; Roach, A. G.; Berghmans, S., Zebrafish: an emerging technology for in vivo pharmacological assessment to identify potential safety liabilities in early drug discovery. British journal of pharmacology 2008, 154 (7), 1400-13.
40. Mimeault, M.; Batra, S. K., Emergence of zebrafish models in oncology for validating novel anticancer drug targets and nanomaterials. Drug discovery today 2013, 18 (3-4), 128-40.
41. Zhao, C.; Yang, H.; Shi, H.; Wang, X.; Chen, X.; Yuan, Y.; Lin, S.; Wei, Y., Distinct contributions of angiogenesis and vascular co-option during the initiation of primary microtumors and micrometastases. Carcinogenesis 2011, 32 (8), 1143-50.
42. Stoletov, K.; Kato, H.; Zardouzian, E.; Kelber, J.; Yang, J.; Shattil, S.; Klemke, R., Visualizing extravasation dynamics of metastatic tumor cells. Journal of cell science 2010, 123 (Pt 13), 2332-41.
43. Gaudenzi, G.; Albertelli, M.; Dicitore, A.; Wurth, R.; Gatto, F.; Barbieri, F.; Cotelli, F.; Florio, T.; Ferone, D.; Persani, L.; Vitale, G., Patient-derived xenograft in zebrafish embryos: a new platform for translational research in neuroendocrine tumors. Endocrine 2017, 57 (2), 214-219.
44. Wu, J. Q.; Zhai, J.; Li, C. Y.; Tan, A. M.; Wei, P.; Shen, L. Z.; He, M. F., Patient-derived xenograft in zebrafish embryos: a new platform for translational research in gastric cancer. Journal of experimental & clinical cancer research : CR 2017, 36 (1), 160.

Supplementary Files

This is a list of supplementary files associated with this preprint. Click to download.

- Supplementary.pdf